PAPER

Dual-functionalised shellac nanocarriers give a super-boost of the antimicrobial action of berberine†

Saba S. M. Al-Obaidy, [ID] Gillian M. Greenway [ID] and Vesselin N. Paunov [ID] *

We have developed highly efficient antimicrobial nanocarriers for berberine (BRB) based on shellac nanoparticles (NPs) which were surface-functionalised with a surface active polymer, Poloxamer 407 (P407), and the cationic surfactant octadecyltrimethylammonium bromide (ODTAB). These shellac nanocarriers were produced in a two-step process which involves: (i) a pH change from aqueous ammonium shellac solution using P407 as a steric stabilizer in the presence of berberine chloride, and (ii) addition of ODTAB to yield shellac nanocarriers of cationic surface. We determined the BRB encapsulation efficiency and release profiles from such nanocarriers. We explored the antimicrobial action of these nanocarriers at different stages of their preparation which allowed us gain better understanding how they work, fine tune their design and reveal the impact of the nanoparticle coatings on to its antimicrobial effect. The antimicrobial action of BRB loaded within such shellac NPs with cationic surface functionality was examined on three different microorganisms, *C. reinhardtii*, *S. cerevisiae* and *E. coli* and compared with the effect of free BRB as well as non-coated BRB-loaded nanocarriers at the same BRB concentrations. We found that the cationic surface coating of the shellac NPs strongly amplified the efficiency of the encapsulated BRB across all tested microorganisms. The effect was attributed to the increased attraction between the ODTAB-coated BRB-loaded NPs and the anionic surface of the cell walls which delivers locally high BRB concentration. This nanotechnological approach could lead to more effective antimicrobial and disinfecting agents, dental formulations for plaque control, wound dressings, antialgal/antibiofouling formulations and antifungal agents.

Introduction

Nanocarrier systems have been widely developed in the pharmaceutical industry due to their ability to control the release of drugs for efficient delivery.[1] Recently, nanocarriers formulated from biodegradable materials have attracted much attention following concerns about the post-use fate of the nanocarrier formulations.[2,3] Environmentally biodegradable NPs from renewable natural materials such as lignin, cellulose and shellac could have a wide range of industrial and pharmaceutical applications. Frangville *et al.*[4] developed biodegradable lignin nanoparticles which showed no measurable toxicity against proxy organisms such as yeast and microalgae. Recently, these were applied in a delivery system based on Ag⁺-loaded lignin NPs which were coated with a cationic polyelectrolyte.[5,6] Al-Awady *et al.*[7] demonstrated that the nanotoxicity of polyelectrolyte-coated NPs alternates with the surface charge where the particles with a cationic outer layer are much

more toxic than the ones with an outer layer of anionic polyelectrolyte.

Berberine (BRB) is an isoquinoline alkaloid (Fig. 1B) which can be found in the roots, rhizome, and stem barks of a number of commonly therapeutic plant species such as *Berberis vulgaris*, *Hydrastis canadensis*, *Coptis chinensis*, *Arcangelisia flava*, *B. aquifolium* and *B. aristata*.[8] A range of studies indicate that BRB possesses many significant pharmacological and biological activities, including antimicrobial, anti-helminthic, anti-inflammatory, and anti-oxidative effects.[9–11] It has been suggested that BRB may also have an effect on other diseases such as diabetes, arrhythmia, hypertension, gastrointestinal diseases,[12] and that it is a potential chemotherapeutic agent.[13] Berberine delivery systems based on liposomes, solid lipid nanoparticles and nano-emulsions have been recently explored.[14] Several approaches have been used to prepare BRB-loaded liposomes, such as the active loading method, the thin film evaporation method and a combination of the active loading and thin film evaporation methods.[14,15] Solid lipid nanoparticles (SLNs) loaded with BRB have been prepared from biodegradable solid lipids using a mixture of lipid materials, showing good stability with a mean size of 77 nm and a BRB loading percent of 4.2%. BRB–SLNs at high dose (100 mg kg⁻¹)

Department of Chemistry and Biochemistry, University of Hull, Hull, HU67RX, UK. E-mail: v.n.paunov@hull.ac.uk; Fax: +44 (0)1482 466410; Tel: +44 (0)1482 465660

† Electronic supplementary information (ESI) available. See DOI: 10.1039/c8na00121a

showed more potent effects when compared to an equivalent dose of BRB.[16] Using a high-pressure homogenization method,[17] BRB was loaded within SLNs using glyceryl monostearate with a drug entrapment efficiency of ~70 and loading drug ratio of 2.85.

BRB-loaded SLNs showed significant inhibition *in vitro* for breast cancer MCF-7 cells, HepG 2, and A549 cancer cells.[18] Khemani *et al.*[19] loaded BRB onto polylactide glycolic acid nanoparticles using biodegradable poly(D,L-lactide-*co*-glycolide) with ratio of a 75 : 25 by single emulsion as well as multiple emulsion solvent evaporation techniques with BRB encapsulation of 65%. Another study reported BRB-loaded *O*-hexadecyl-dextran NPs which were evaluated for their cyto-protective efficacy in high glucose stressed primary hepatocytes and these showed much higher efficiency than free BRB in inhibiting high glucose induced oxidative stress, mitochondrial depolarization and downstream events of apoptotic cell death.[20] Al-Awady *et al.*[21] developed antimicrobial particles based on BRB encapsulated in surface-functionalised nanogels.

Shellac is the refined product of the natural material Lac secreted by the small parasitic insect *Kerria lacca* on different host trees in South Eastern Asia. It has numerous applications in agriculture, food products and enteric coatings for tablets,[22] lacquers,[23,24] dental baseplates,[25,26] dental varnishes[27,28] coating and matrix material,[23,29,30] additive in foods and cosmetic products, encapsulating agent in pharmaceuticals,[31–33] as well as a moisture barrier coating for fruits and vegetables.[34,35]

Shellac is a complex mixture of polar and non-polar components consisting of polyhydroxyl acids, lactones and anhydrides,[36–38] it has a pK_a of 6.9 to 7.5 and it is acid resistant,[39] being practically insoluble in acidic to neutral aqueous medium (pH < 7).[31,40,41] Colloidal shellac dispersions have been reported in literature for coating purposes, precipitated from alcoholic shellac solution in distilled water.[42] Colloidal shellac with particle size 150–300 nm was formulated by Patel *et al.*[43] for silibinin encapsulation by using an anti-solvent method and xanthan gum as stabilizer. Kraisit *et al.*[44] used chitosan as stabilizer to prepare shellac suspensions with size range 100–300 nm for encapsulation of bovine serum albumin. Krause and Müller[45] reported preparation of an aqueous shellac dispersion using high pressure homogenisation technique, although the obtained particle size was rather large (~5 μm). We present a more comprehensive comparison of BRB nanocarriers in the ESI (Table S1†).

In the present study, we combine some of these ideas to develop an ultra-efficient BRB nanocarrier for antimicrobial applications based on biocompatible surface functionalised shellac NPs. Fig. 1A explains the steps of the encapsulation of BRB into the shellac nanocarriers and their surface functionalisation. The retention of the BRB in the core of the nanogel is based on hydrophobic and electrostatic interactions within the shellac matrix of the nanocarrier particles. Here we report dual-functionalised nanocarriers for BRB based on sterically stabilised shellac NPs with a cationic surface functionality which
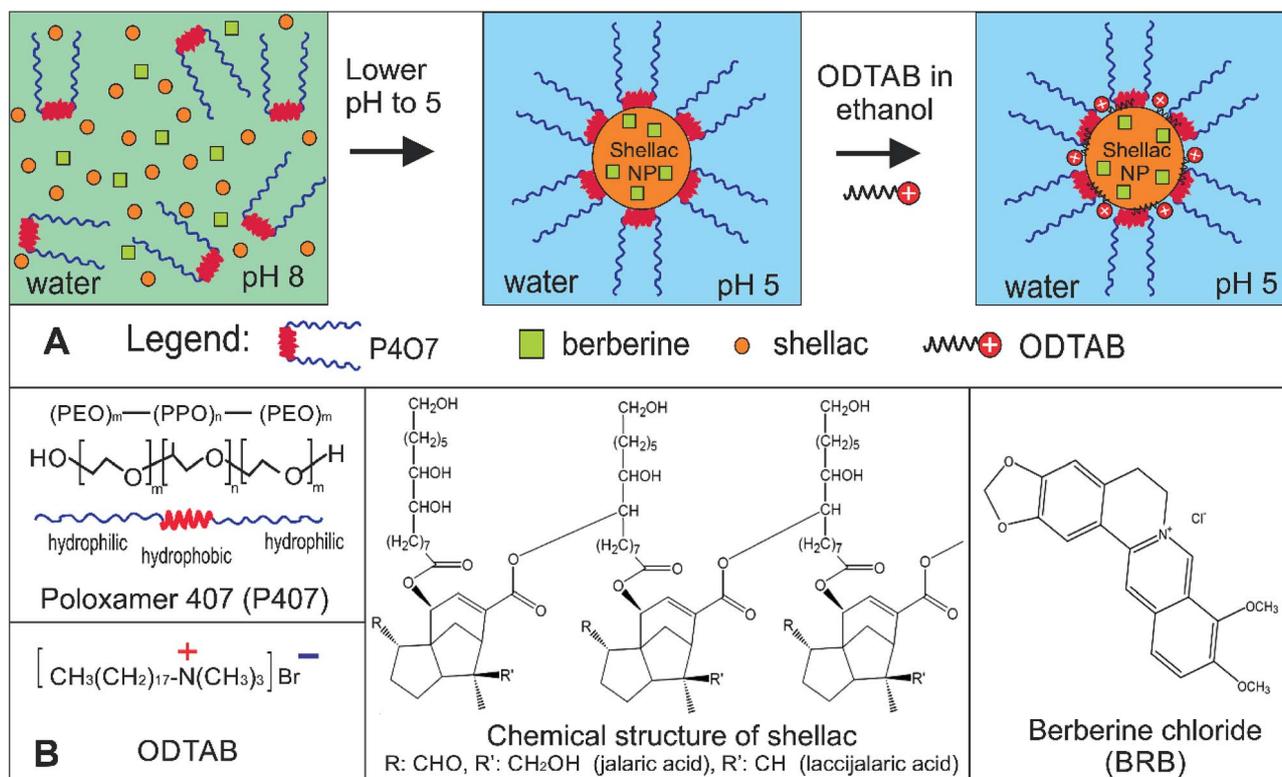

Fig. 1 (A) Schematics of the two step process for preparation of shellac nanocarriers for berberine with cationic surface functionality by steric stabilisation with Poloxamer 407 (P407) and doping with the cationic surfactant octadecyltrimethylammonium bromide (ODTAB). (B) Molecular structures of the constituting materials for preparation of antimicrobial shellac nanocarriers for berberine (BRB): Poloxamer 407 (P407), octadecyltrimethylammonium bromide (ODTAB), shellac and berberine chloride.

have a long shelf life and are also able to strongly adhere to microbial cell walls.

This was done by using a surface active tri-*block*-copolymer, Poloxamer 407 (see Fig. 1), which sterically stabilised the formed shellac NPs suspension and enabled us to develop very small shellac NPs loaded with BRB in one preparation step. However, achieving cationic surface functionality of the nano-carrier required doping of the pre-formed sterically stabilised shellac NPs suspension with an ultra-low concentration of a water-insoluble cationic surfactant (ODTAB) – see Fig. 1. The choice of ODTAB was justified as it allows direct adsorption on the shellac NPs surface while the already formed P407 layer in the first step remains intact. This strategy proved very successful, as the carrier maintained its steric stability while being surface charge-reversed by secondary coating with ODTAB. We studied the antibacterial, anti-fungal and antialgal action of the BRB-loaded shellac NPs compared with free BRB on three proxy microorganisms, *C. reinhardtii*, *S. cerevisiae* and *E. coli*, respectively. We also studied the BRB release kinetics and the boost of its antimicrobial action before and after surface functionalising of the shellac NPs with ODTAB. We show that this strategy can strongly amplify the antimicrobial action of BRB compared to solutions with an equivalent concentration of free BRB or the non-loaded nanocarrier.

Materials and methods

Materials

Shellac was used in a soluble form as the ammonium salt at pH > 7, the alkaline solution was a gift from (Stroever Schellack Bremen, Germany) and is commercially available as SSB Aqua Gold™ (solid content 25%). Poloxamer 407 (purified), berberine chloride (98%), and 3′,6′-diacetyl fluorescein (FDA), were obtained from Sigma-Aldrich ltd. UK. Octadecyl-trimethylammonium bromide (ODTAB) was supplied by Fluka Chemika, UK. The BacTiter-Glo Microbial Cell Viability Assay was purchased from Promega, UK. *Chlamydomonas reinhardtii* (cc-124 strain) was kindly provided by Flickinger group from North Carolina University, USA. This microalgae culture was grown in Tris-Acetate-Phosphate (TAP) culture medium and incubated at a temperature of 30 °C. The *C. reinhardtii* culture media consisted of TAP salts (NH_4Cl; $MgSO_4 \cdot 7H_2O$ and $CaCl_2 \cdot 2H_2O$), phosphate buffer solution (PBS) and Hutner's trace elements solution (EDTA disodium salt, $ZnSO_4 \cdot 7H_2O$, H_3BO_3, $MnCl_2 \cdot 4H_2O$, $CoCl_2 \cdot 6H_2O$, $CuSO_4 \cdot 5H_2O$, $FeSO_4 \cdot 7H_2O$, $(NH_4)_6$-$Mo_7O_{24} \cdot 4H_2O$, all purchased from Sigma-Aldrich, UK). The microalgae batch was grown in the TAP media at pH 7 while being illuminated for 72 hours with a white luminescent lamp with a light intensity of 60 W m^{-2} under constant stirring with a magnetic stirrer.[12,13,46]

The stock cultures of *C. reinhardtii* were with typical concentration 4×10^5 cells per mL determined by cell counter (Nexcelom Cellometer Auto X4) and the *E. coli* bacterial culture stock was with approximately 5×10^7 cells per mL. *Saccharomyces cerevisiae* (Baker's yeast), was purchased from Sigma-Aldrich. It was cultured by hydrating 10 mg of lyophilized yeast cells in 10 mL Milli-Q water. Then 1 mL of this hydrated suspension was added to 100 mL of autoclaved YPD culture media[47] consisting of peptone (Sigma Aldrich, UK), D-glucose, (Fisher Scientific, UK), and yeast extract, (Oxoid ltd, UK.), then incubated at 30 °C for 24–48 hours. *Escherichia coli*, sourced from Thermofisher (Invitrogen MAX Efficiency™ DH10B™) was kindly provided for our antibacterial tests by Prof Rotchell's group at the University of Hull, UK. The cells were cultured in autoclaved Luria–Bertani medium (LB medium)[47,48] prepared by dissolving 0.5 g yeast extract, 0.5 g sodium chloride (Sigma Aldrich), and 1 g tryptone (Oxido ltd), in 100 mL water. Fluorescein diacetate (FDA, 98%) for cell viability assays was supplied from Sigma Aldrich, UK. Deionised water purified by reverse osmosis and ion exchange from a Milli-Q water system (Millipore, UK) was used in all our studies. Its surface tension was 71.9 mN m^{-1} at 25 °C, with measured resistivity less than 18 MΩ cm^{-1}.

Preparation of shellac NPs and loading with BRB

Shellac NPs were prepared by mixing 0.25 w/v% of ammonium shellac salt and BRB solution at pH 8 with different concentrations of P407 and then lowering the solution pH to 5 by adding drop-wise 0.01 M HCl with agitation. Different concentrations of BRB were used in a mixture of shellac and P407 with a constant ratio of 0.25 wt% : 0.2 wt%, respectively.

Cationic surface functionalization of the BRB-loaded shellac NPs

In order to promote their adhesion to the negatively charged microbial cell walls, the shellac NPs surface charge was reversed from negative (P407-stabilised shellac NPs loaded with BRB) to positive by additional coating with the cationic surfactant ODTAB. Typically, 0.03 wt% of BRB loaded in 0.25 wt% shellac NP was coated with varied concentrations of ODTAB (delivered to the shellac NP suspension by drop-wise addition from 3% ODTAB in ethanol at constant stirring).

Shellac NPs size, zeta-potential and morphology characterisation

The particle size distribution and zeta-potential of the shellac NPs with and without BRB were measured by the dynamic light scattering (DLS) technique using a zeta sizer Nano ZL (Malvern Instrument Ltd, UK). All measurements were carried out in triplicates. Morphological examination of the nanoparticles was performed by transmission electron microscopy (TEM) (Joel 2010, Japan), a few drops of the sample were placed on carbon-coated copper grids and negatively stained with 1% aqueous uranyl acetate. Once air dried, the sample was imaged with a Gatan Ultrascan 4000 digital camera attached to the Jeol 2010 TEM running at 200 kV.

Fourier transform infrared (FTIR) and UV-vis spectroscopy study

FTIR spectroscopy (Thermo Scientific Nicolet 380 FT-IR, Hemel Hempstead, UK) was used to characterise the shellac NPs and BRB-loaded shellac NPs. This technique was also used to

confirm the adsorption of P407 on shellac NPs surface and the intercalation between the BRB and the shellac molecules. In order to confirm the loading percentage of BRB within the shellac NPs a UV-vis spectrophotometry technique was used. A sample of BRB-loaded shellac NPs was dissolved in alkaline solution (pH 8) and the spectrum was recorded between 220–700 nm using spectrophotometer (model Bio Lambda 10, USA). Same spectra were recorded at the same range for shellac, P407 and free BRB.

Encapsulation efficiency and BRB loading contents in shellac NPs

The encapsulation efficiency and the drug loaded content was indirectly calculated by measuring the absorbance of the non-encapsulated drugs. The non-encapsulated BRB solution was filtered using a 20 nm syringe filter and the absorbance of this filtered BRB solution was measured at 422 nm using UV-vis spectrophotometer (model Bio Lambda 10, USA). Calibration curve of BRB was made by measuring the absorbance of a series of standard BRB solutions. The BRB loading contents and encapsulation efficiency were calculated as shown below[49]

$$\text{Encapsulation efficiency } (\%) = \frac{[\text{total drug} - \text{unencapsulated drug}]}{[\text{total drug}]} \times 100$$

$$\text{Drug loading content } (\%) = \frac{[\text{total drug} - \text{unencapsulated drug}] \times 100}{[(\text{total drug} - \text{unencapsulated drug}) + \text{shellac} + \text{poloxamer amount}]}$$

In vitro BRB release kinetics from shellac NPs

The dialysis method was used to determine the in vitro BRB release profile from the shellac NPs. 50 mL of the sample containing of BRB-loaded shellac NPs were dialyzed. A dialysis bag of 12–14 K MWCO with pore diameter 2.5 nm was immersed in a 500 mL buffer phosphate solutions (for pH 5.5 and 7.4). The bag was stirred gently with an orbital shaker at 37 °C temperature and 100 rpm. At specific time intervals, 2 mL of the dialysis solution was taken and analysed by measuring the UV-vis absorbance from 200 to 700 nm. The measurements were taken at 15, 30, 60, 120, 180, 240, 300, 360 and 1440 minutes. All release experiments were carried out in triplicates. The percentage of cumulative drug release was calculated using the equation shown below[50]

$$\% \text{ in vitro BRB release} = \frac{M_{\text{released}}}{M_{\text{total}}} \times 100,$$

where M_{released} is the amount of BRB released from the shellac NPs at time t and M_{total} is the amount of BRB loaded.

Antimicrobial activity of the non-coated BRB-loaded shellac NPs

To study their antimicrobial action, different concentrations of the non-coated BRB-loaded shellac NPs and ODTAB-coated

BRB-loaded shellac NPs stock suspensions were mixed with fixed aliquots of the microbial cells for various incubation times. The cells were removed from their original growth media and transferred in Milli-Q water. Blank shellac NPs without BRB (as a negative control) and free BRB aqueous solution (positive control) was incubated as with equivalent cell samples for the same durations. The cell viability of C. reinhardtii and yeast was measured using a cell counter after incubating 1 mL of the treated cells (washed from the shellac NPs formulation), with 10 μL of 0.1% FDA in acetone for 10 minutes and washing with Milli-Q water by centrifugation. The viability of E. coli was measured after incubating the cells with the BRB-loaded shellac NPs. 100 μL of the treated E. coli suspension was washed and mixed with 100 μL of BacTiter-Glo™ cell viability reagent in white opaque 96-well microplate and shaken for 5 minutes. The bioluminescence intensity was then measured using a BMG LABTECH instrument (FLUOstar Omega, Germany).

Protocol for SEM imaging of the treated cell samples

The cells were washed with Milli-Q water 3 times to remove the residual NPs by centrifugation at 3000 rpm for 3 minutes. The cell sample was deposited on dry Aclar™ sheets or poly-lysine coated glass coverslips, fixed with 2.5 w/v% glutaraldehyde for 2 hours, followed by washing with cacodylate buffer. The cells were post fixed for 1 hour in 1 wt% osmium tetroxide, washed with a cacodylate buffer, then rinsed with serial ethanol–water solutions starting from 50% ethanol moving up to absolute ethanol, then dried using a critical point dryer. Finally, the samples were coated with carbon (~10 nm) in an evaporator and imaged using scanning electron microscope SEM (ZEISS EVO 60 EP-SEM, Germany).

Results and discussion

Preparation and characterisation of BRB-loaded shellac NPs

The stable shellac nanoparticles were prepared based on a steric repulsion mechanism using P407, a surface active polymer, as stabilizer and the adjustment of the pH from 8 to 5. P407 is a non-ionic co-polymer made up of poly(ethylene oxide) (PEO)–poly(propylene oxide) (PPO) poly(ethylene oxide) (PEO) (see Fig. 1B), which has been widely used in pharmaceutical formulations as a surfactant, solubilizing agent, emulsifying and dispersing agent.[51] The P407 polymer performed very well in sterically stabilizing the shellac NPs due to its amphiphilic nature and the fact that the hydrophobic PPO block adsorbs on the hydrophobic shellac surface attaching two PEO chains (per P407 molecule) on the particle surface (see Fig. 1A). The steric repulsion between these chains on the surface of the shellac NPs leads to their stabilisation. Fig. 2A and B and show the particle size distribution and the zeta potential of shellac NPs formed by mixing 0.25 wt% of shellac with 0.2 wt% P407 at pH 5. The results show narrow particle size and zeta-potential distributions with an average shellac particle size of 66 ± 5 nm and zeta-potential of −18 ± 8 mV. Fig. 2E shows the dependence of the average particle size and zeta potential on the pH of the solution. One can see that the particle size is insensitive to pH as the shellac particles are sterically stabilised,
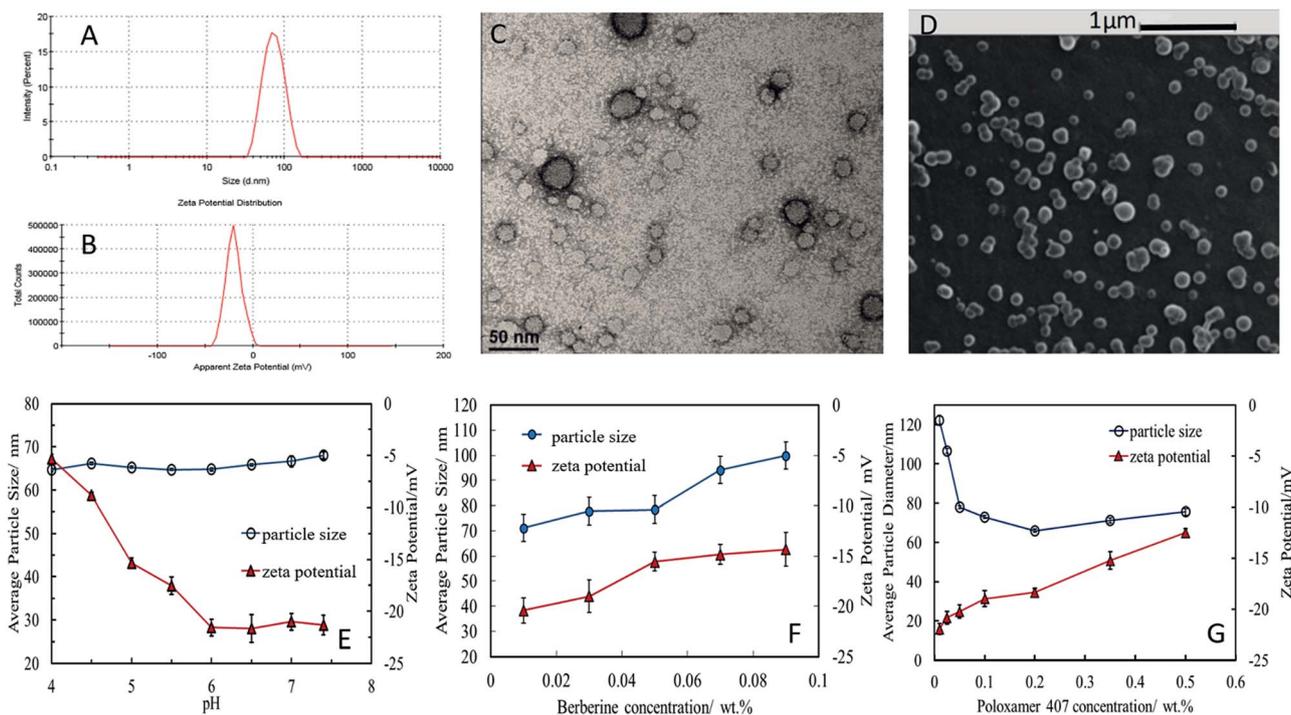
Fig. 2 (A) Particle size and (B) zeta-potential distribution of shellac nanoparticles was obtained by mixing a ratio of 0.25 : 0.2 wt% of ammonium shellac: P407 from pH 8 to pH 5 in Milli-Q water. (C) TEM and (D) SEM image of ODTAB-coated BRB-loaded shellac NPs; (E) the shellac NPs average diameter and zeta-potential as a function of the pH of the media. (F) The effect of the loading BRB concentration on the size of shellac NPs produced using 0.25 wt% ammonium shellac at pH 5 and 0.2 wt% P407. (G) The average size and zeta potential of shellac NPs obtained by adding 0.25 wt% ammonium shellac solution (pH 8) to solutions of different P407 concentrations in Milli-Q water at pH 5.

while the zeta-potential is negative due to the dissociation of the COOH groups of the shellac constituents. Note that here no ODTAB was used to coat these shellac NPs. We used SEM and TEM imaging to explore the morphological characteristic of shellac NPs, BRB-loaded shellac NPs, and ODTAB-coated BRB-loaded shellac NPs, as can be seen in Fig. 2D and E, respectively. The images show that the shape of the shellac NPs is spherical with size less than 50 nm for uncoated particles and less than 100 nm for the coated NPs. We have also used the TEM images of the shellac NPs to measure the particle size distribution and present the results in the ESI file, as shown in Fig. S2,† which also agrees with Zetasizer measurements at pH 5 (see Fig. 2A). Fig. 2F shows that the size of the shellac NPs increased with increasing of BRB loading concentration. Note that the zeta-potential of the BRB-loaded shellac NPs decreased slightly as the BRB loading concentration increased due to the electrostatic attraction between the carboxylic groups of the shellac constituents and the BRB cations.

Fig. 2G shows the average size and the zeta potential of the shellac NPs at different concentrations of P407. The particle size remains fairly constant above 0.2 wt% P407 while the zeta-potential decreases slightly due to the offsetting of the surface by the PEO chains of the attached P407 layers.

FTIR and UV-vis spectroscopy studies

The infrared absorption spectra of shellac, P407, BRB, shellac nanoparticles, and BRB-loaded shellac NPs are represented in

Fig. 3A, the spectrum of shellac (blue line) shows a main broad peak at 3319 cm^{-1} which relates to the absorption of the O–H stretching vibration band, and a peak at 1707 cm^{-1} representing the carbonyl stretching vibration band (C=O) along with a C–O stretching band appearing at 1247 cm^{-1}.[39,52] The P407 spectrum (black line) shows a principal absorption peaks at 2878 cm^{-1} for C–H aliphatic stretching and at 1342 cm^{-1} for the absorption of OH (in-plane O–H bend), another principal peak can be observed at 1097 cm^{-1} which can be assigned to the C–O stretch.[53] Apart from some slight shifts in peaks the IR spectrum of the shellac nanoparticles (brown line) shows no difference to P407 or shellac spectrum.

Some of the P407 peaks were merged with shellac peaks as there is no chemical reaction between shellac and P407, the attraction is an adsorption of the hydrophobic part of P407 on shellac surface, and O–H stretching band still exist at 3392 cm^{-1}, while the carbonyl stretching vibration (C=O) and C–O stretching bands appears at 1711 cm^{-1} and 1241 cm^{-1} respectively. The infrared spectrum of free BRB (red line) is characterised by a principal peak at 1602 cm^{-1} relating to the –C=N– quaternary iminium ion, and a peak at 1504 cm^{-1} (C=C stretching vibration of aromatic ring).[54] The intensity of these peaks declined when BRB was loaded into shellac nanoparticles and most BRB peaks overlap with the shellac NPs bands, this proves the reaction between BRB and shellac, the broad band for O–H stretching seen for shellac still exists although it has shifted slightly as can be seen in Fig. 3A (green line). The BRB content within the nanoparticles was also proved by using UV-vis
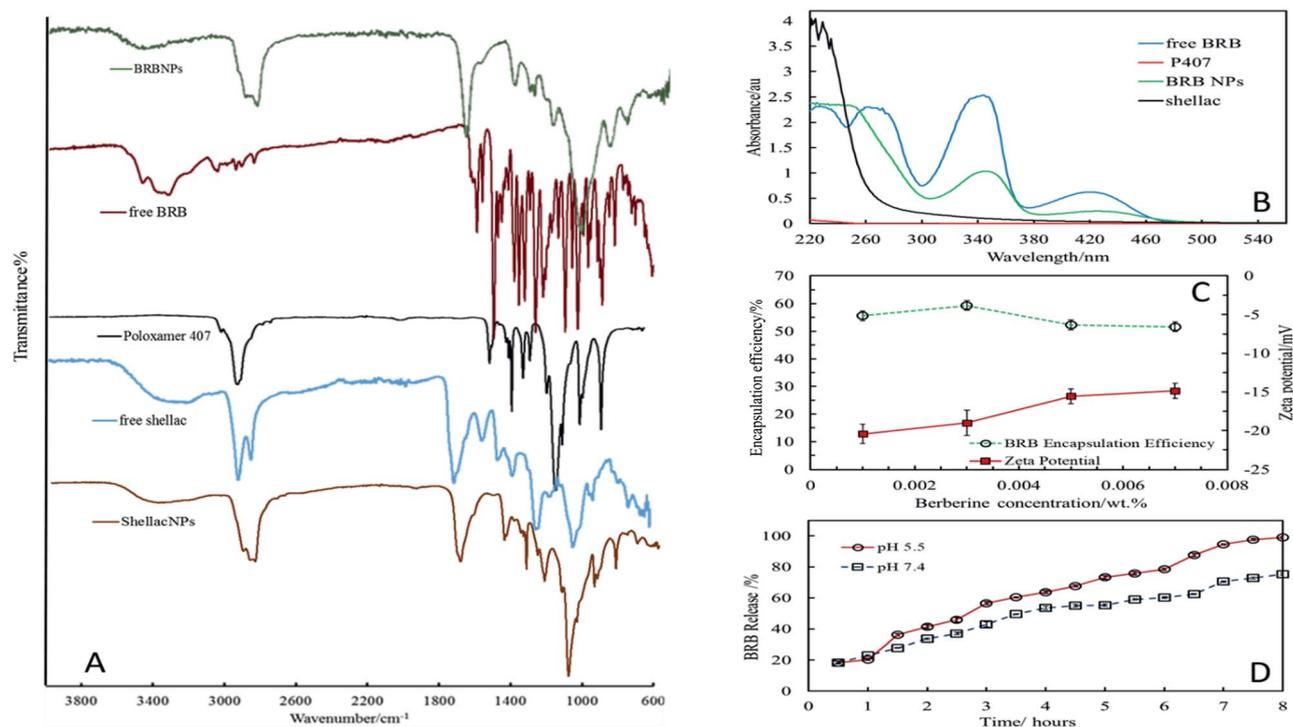
Fig. 3 (A) Fourier Transform Infra-Red (FTIR) spectra of BRB−NPs, free BRB, P407, shellac ammonium salt (free shellac), and Shellac NPs; (B) UV-vis absorption spectrum of BRB, free shellac, non-coated BRB-loaded shellac NPs and P407; (C) the encapsulation efficiency percentage of different concentrations of BRB-loaded shellac NPs at pH 5, and (D) the percentage of *in vitro* BRB release as a function of time at different pH.

spectroscopy technique. Fig. 3B shows the UV-vis absorption spectra of shellac, P407, free BRB and BRB-loaded shellac NPs. The shellac spectrum (black line) shows random peaks at 220–300 nm due to its different carboxylic acid components without a significant maximum wavelength, while the free BRB (blue line) has four absorption peaks, one which was in the visible area with a wavelength of 422 nm and three peaks in the UV region with wavelengths at 350 nm, 265 nm and 230 nm, respectively. These spectra show that there is no spectral interference between the absorbance of shellac, BRB and P407 (which has no significant peak between 220–700 nm, red line). The green line is the absorbance spectrum for the BRB-loaded shellac NPs (BRB NPs) where it can be clearly seen that two peaks appear at 422 and 350 nm belonging to BRB with no specific peaks around wavelengths 220 and 300 nm due to shellac absorption, this provides a clear evidence that the cationic BRB is conjugated with the anionic carboxyl groups of the shellac constituents.

BRB encapsulation efficiency and release kinetics from shellac NPs

We experimented with different BRB concentrations and BRB : shellac ratios and we report here only the optimal combination which yielded the best encapsulation efficiency. The BRB encapsulation efficiency within the NPs was measured at pH 5. It was found that the highest encapsulated amount of BRB within shellac nanoparticles was about 60% at the following composition, 0.03 wt% : 0.25 wt% : 0.2 wt% of BRB : shellac : P407 respectively, as shown in Fig. 3C. The *in vitro* release profile measurement of BRB from shellac NPs was

carried out in PBS at pH 5.5 and 7.4. Fig. 3D shows the BRB release profile which was higher at acidic pH 5.5, and reached 100% after 8 hours, while at pH 7.4 the maximum released BRB was about 75% after 8 hours.

The cytotoxicity effect of non-loaded shellac NPs

In order to determine whether the loading of BRB within shellac nanoparticles could enhance the antibacterial activity of BRB, the cytotoxic effect for each component of the nanocarrier, was studied on representative microalgae, yeast and bacterial cells. The cytotoxic assay of shellac NPs was determined by incubation of the cells with shellac NPs suspensions of different shellac concentrations produced by serial dilutions of more concentrated stock. The cells were removed from the culture media to avoid any interaction between the shellac NPs and the media components. Fig. 4 shows the cytotoxic effects of shellac NPs without BRB on *C. reinhardtii*, *S. cerevisiae* and *E. coli*, respectively. As it can be seen from Fig. 4A, there is a small effect of shellac NPs on the algal cells at relatively high concentration due to the antibacterial properties of P407, which was used as a stabilizer. It has been previously reported that P407 might create a adsorption layer on the microbial cell surface,[55–57] so the combination between P407 and the shellac NPs may play a synergistic antimicrobial role within this nanocarrier design. The shellac NPs, however, showed no pronounced effect when incubated with yeast and *E. coli* for 6 hours, as demonstrated in Fig. 4B and C. One possible explanation for the lack of effect on yeast is that its cells have much a thicker cell wall which mitigates the effect of P407 at these
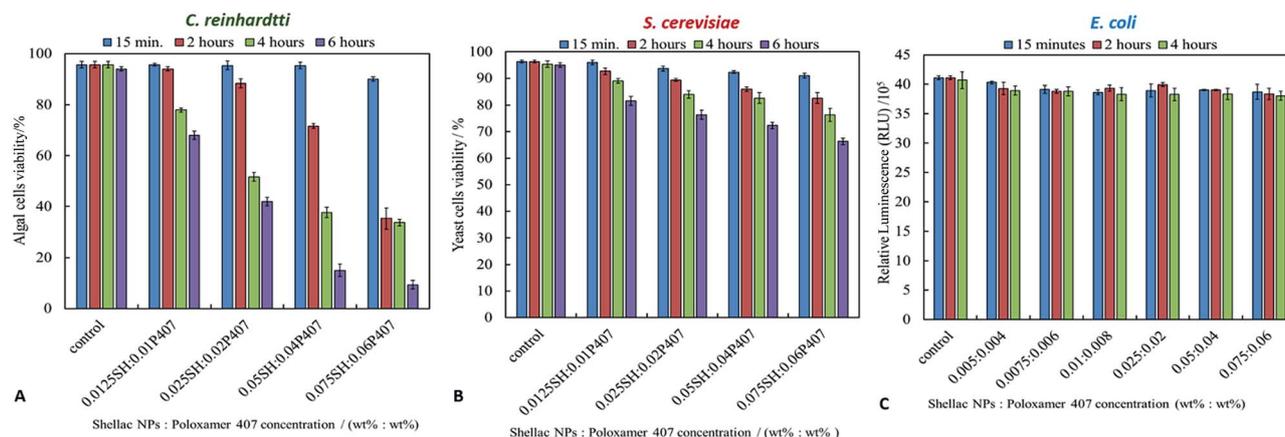
Fig. 4 The effect of the P407 stabilised non-loaded shellac NPs on the viability of (A) *C. reinhardtii*, (B) *S. cerevisiae* and (C) *E. coli* cells incubated with different concentrations of shellac NPs (made from fixed ratio of 0.25 wt% ammonium shellac and 0.2 wt% P407) at different incubation times. The ratios on the *x*-axis show the actual concentrations of both shellac and P407. No BRB was used in these experiments. Here the shellac NP were stabilised by P407 but not coated with ODTAB.

concentrations. For all cell types studied, at lower concentration the shellac NPs are benign over the duration of the experiment (4 hours).

Antimicrobial activity of BRB-loaded shellac NPs

We compared the antimicrobial activity of free BRB and BRB-loaded shellac NPs on the same microbial cultures, *C. reinhardtii*, *S. cerevisiae* and *E. coli*, in order to determine whether the loading of BRB within the shellac NPs could enhance its antimicrobial activity. The purpose of encapsulating BRB within shellac NPs was to increase the antimicrobial action of BRB. This was achieved due to the increased surface area of the nanocarrier, resulting in the need for less antimicrobial, thus reducing the potential side effects of the drug. Furthermore the BRB encapsulation increases the BRB local concentration which leads to enhance stability and the bioavailability in medical formulations increasing its efficacy.[58–62] Fig. 5 shows the cell viability of the *C. reinhardtii* as a function of the concentration of free BRB. The experiment shows that after incubation for 15 minutes with 0.01 wt% and 0.05 wt% free BRB, the viability of the algal cells is reduced instantly from 91% (for the control) to 18% and 11%, respectively. After 2 hours of incubation, the algal cells viability rapidly declined from 90% (for the control) to be 3% at 0.01 wt% of free BRB, while at 0.05 wt% all algal cells were killed. The cell viability kept reducing as the incubation time increased, and after 6 hours most cells died at free BRB concentrations of 0.007 wt% or higher. These findings are consistent with the literature reports[63] that BRB is an effective antimicrobial agent at reasonably low concentrations over sufficiently long period of time. Correspondingly, we studied the cytotoxicity of non-coated BRB-loaded shellac NPs on the same algal cells. As it was shown previously, that BRB can be efficiently encapsulated within shellac NPs up to 60% with the release reaching up to 100% of the total amount of BRB at pH 5.5 after 6 hours. Fig. 5B shows the effect of different concentrations of BRB-

loaded shellac NPs on the algal cell viability at room temperature up to 6 hours. However, after 15 minutes incubation, the algal cells appeared to be not significantly affected by the BRB-loaded shellac NPs as the viability was reduced slightly to 77% at 0.01 wt% BRB–Shellac NPs in comparison with the control which was 92%. The latter represents the viability of algal cells alone in a solution of pH 5.5. After 6 hours of incubation the viability of the cell decreased slightly, at 0.007 wt% and 0.01 wt% of BRB-loaded in shellac NPs, the cell viability decreased to be 6% and 1.5% respectively. The corresponding SEM images of the treated algal cells revealed a good evidence for the effect of free BRB and BRB encapsulated within shellac NPs on the cells after 4 hours of incubation. Fig. 5E and F shows that the morphology of the algal cells has changed from relatively smooth and round (Fig. 5C and D) to irregular shapes after incubating with 0.01 wt% free BRB and most algal cells lose their flagella compared with the control sample (Fig. 5C and D). Interestingly, the algal cells incubated with BRB-loaded shellac NPs for the same period and overall BRB concentration (Fig. 5G and H), were not visibly affected. One possible explanation for the reduced performance of the BRB-loaded in shellac NPs is that the nanocarrier particles loaded with BRB still maintain their negative surface charge which caused a electrostatic repulsion between them and the negatively charged algal cell membrane. This reduces the overall effect of BRB as most of it remains encapsulated in the nanocarrier without direct contact with the cells.

We also performed similar experiments with *S. cerevisiae* for comparison of the effect of free BRB and non-coated BRB-loaded shellac NPs at the same overall BRB concentration. The results are presented in Fig. 6A for free BRB and Fig. 6B for BRB-loaded shellac NPs. One can see that the free BRB has no significant anti-yeast effect over the studied range of BRB concentrations. However, a much stronger effect is observed with BRB-loaded shellac NPs. One can possible attribute this to the build-up of an adsorption layer of P407-stabilised BRB-loaded shellac NPs which brings some fraction of them in
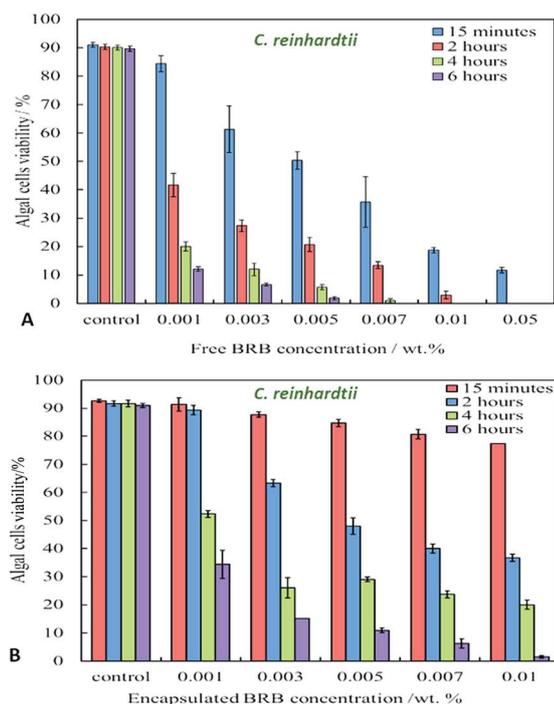
Fig. 5 The viability of *C. reinhardtii* upon incubation at pH 5.5 with aqueous solutions of different concentrations of (A) free BRB and (B) BRB-loaded shellac NPs (non-coated with ODTAB) at room temperature up to 6 hours incubation time at pH 5.5. (C)–(H) SEM images of *C. reinhardtii* whereby (C) and (D) represent the control sample of the microalgae cells. (E) and (F) *C. reinhardtii* incubated with 0.01 wt% free BRB after 4 hours incubation, (G) and (H) *C. reinhardtii* incubated with 0.01 wt% BRB-loaded in shellac NPs up to 4 hours. Note that the free BRB is more effective anti-algal agent than the non-coated shellac NPs with the same concentration of shellac NP-loaded BRB.

close proximity of the yeast cells. This is partially supported by the SEM images of the cells (Fig. 6G and H) where we can identify a limited number of adhering BRB nanocarriers. In the case of free BRB, the yeast cells morphology remains visibly unaffected (Fig. 6E and F) compared with the control sample (Fig. 6C and D). The same type comparison between the anti-bacterial effect of free BRB and BRB-loaded shellac NPs on *E. coli* reveal a result similar to that of the algal cells, as described earlier. Fig. 7A shows that free BRB has a slightly higher anti-bacterial action than the equivalent amount of BRB-loaded in shellac NPs (Fig. 7B). The SEM images of the treated *E. coli* show more significant change in the cells walls morphology for cells treated with free BRB (Fig. 7E and F) compared with the control (Fig. 7C and D) and these treated with BRB-loaded shellac NPs (Fig. 7G and H). The latter show very few BRB nanocarriers remaining on the bacterial cell walls due to the electrostatic repulsion between them.

Antimicrobial effect of free ODTAB and ODTAB-coated non-loaded shellac NPs

We studied the cytotoxicity of the ODTAB and the non-loaded shellac NPs which have been coated with ODTAB (without BRB), on algae, yeast, and bacteria in order to gain better understanding of its contribution towards the antimicrobial efficiency of the coated nanocarrier. Fig. 8A–C show the effect of free ODTAB delivered directly to the cell cultures of the algae, yeast and the bacteria after 15 minutes of incubation. Note that ODTAB alone has very high toxicity at moderate concentrations.

ODTAB is a cationic surfactant but it is practically insoluble in water at room temperature. Since it was delivered in the cell suspension from 1 wt% ODTAB in ethanol solution, one can expect that ODTAB is in particulate form (precipitates) which act as cationic particles and has potentially the ability to disturb the cell membranes, hence its relatively high toxicity. However, at low concentrations ODTAB has limited effect on the cell viability. Fig. 8D–F show the antimicrobial effect of shellac NPs coated with ODTAB on the same microbial cell cultures. It can be seen that the ODTAB-coated nanocarriers (non-loaded) have significantly lower toxicity compared with the equivalent amount of free ODTAB alone. In our nanocarrier design we have chosen the lowest concentration of ODTAB (0.001 wt%) with which to coat the shellac NPs as this does not incur high additional toxicity of the nanocarrier particles themselves. This allowed us to compare the effect of the BRB loading on the nanocarrier antimicrobial action. Fig. 9 shows the SEM images of the three types of microbial cells incubated with non-loaded ODTAB-coated shellac NPs. One can see that there is a significant accumulation of nanocarrier particles on the surface of the cell walls for *C. reinhardtii* (Fig. 9A and B) and *E. coli* (Fig. 9E and F). For the yeast cells (Fig. 9C and D), once can clearly see changes on the yeast cell wall morphology, but no nanocarrier particles have remained attached after the SEM sample preparation (*cf.* with Fig. 6G and H where the nanocarrier is not charged positively). One possible explanation for the different result for yeast is that the cell wall is not sufficiently charged for electrostatic adhesion to retain the particles during the SEM sample preparation.
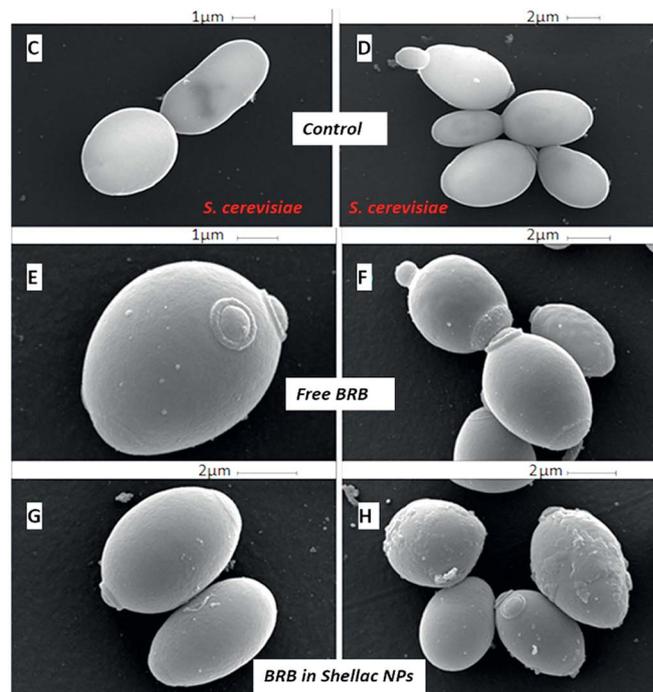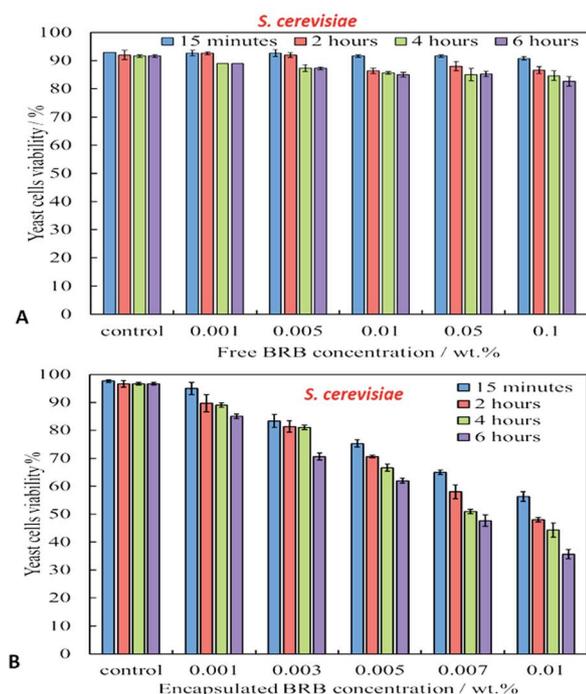
Fig. 6 The viability of *S. cerevisiae* upon incubation at pH 5.5 with aqueous solutions of different concentrations of (A) free BRB and (B) BRB-loaded shellac NPs (non-coated with ODTAB) at room temperature up to 6 hours incubation time at pH 5.5. (C)–(H) SEM images of *S. cerevisiae* whereby (C) and (D) represent the control sample. (E) and (F) *S. cerevisiae* cells incubated with 0.01 wt% free BRB after 4 hours incubation, (G) and (H) *S. cerevisiae* incubated with 0.01 wt% BRB-loaded in shellac NPs up to 4 hours. Note that the free BRB is less effective anti-yeast agent than the non-coated shellac NPs with the same concentration of shellac NP-loaded BRB.
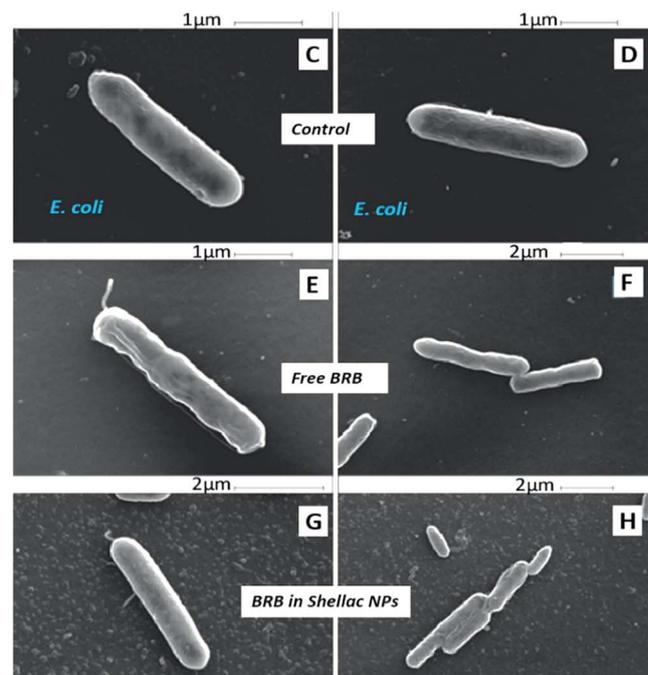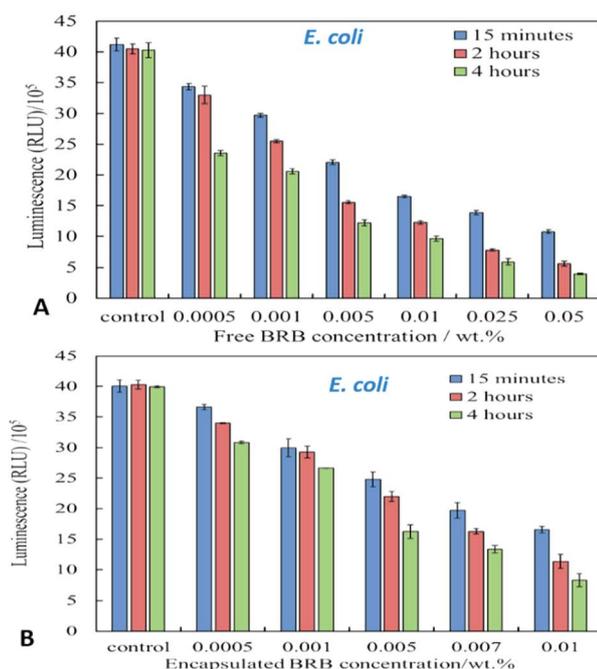

Fig. 7 The viability of *E. coli* upon incubation at pH 5.5 with aqueous solutions of different concentrations of (A) free BRB and (B) BRB-loaded shellac NPs (non-coated with ODTAB) at room temperature up to 6 hours incubation time at pH 5.5. (C)–(H) SEM images of *E. coli* whereby (C) and (D) represent the control sample of the microalgae cells. (E) and (F) *E. coli* incubated with 0.01 wt% free BRB after 4 hours incubation, (G) and (H) *E. coli* incubated with 0.01 wt% BRB-loaded in shellac NPs up to 4 hours. Note that the free BRB is more effective antibacterial agent than the non-coated shellac NPs with the same concentration of shellac NP-loaded BRB.
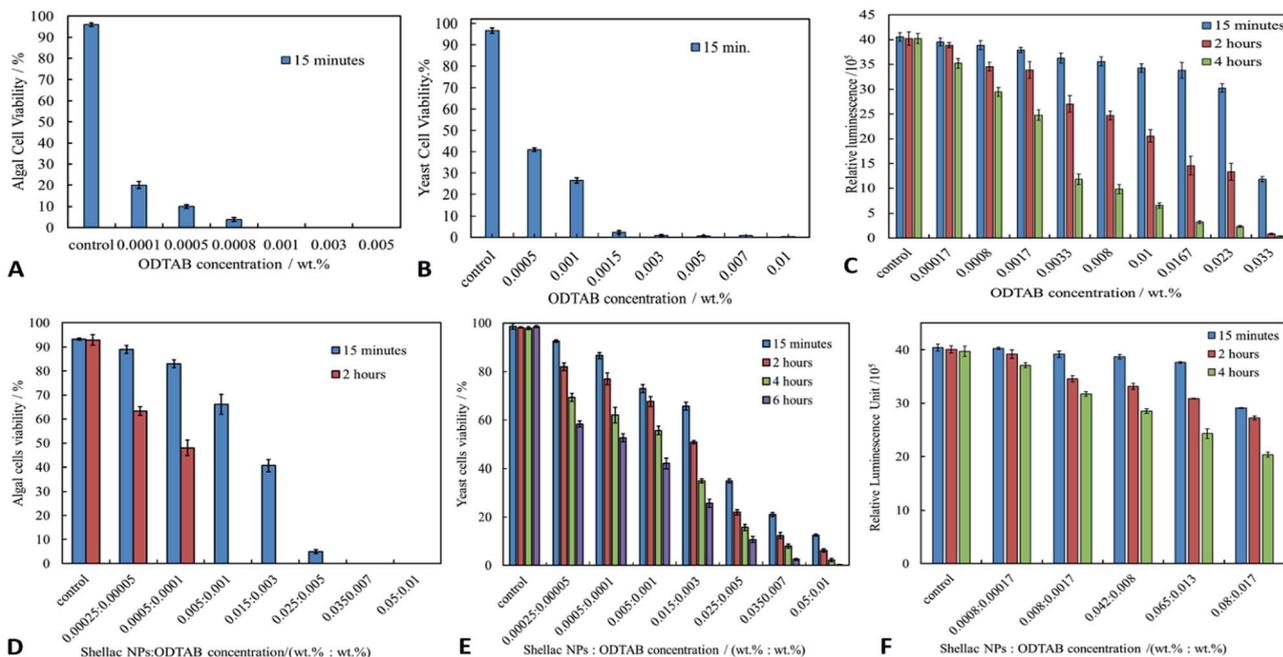
Fig. 8 The cytotoxic effect of solutions of different ODTAB concentrations on (A) *C. reinhardtii*, (B) *S. cerevisiae* and (C) *E. coli* for several different incubation times at room temperature. The cytotoxic effect of non-loaded ODTAB-coated shellac NPs of different concentrations on (D) *C. reinhardtii*, (E) *S. cerevisiae* and (F) *E. coli* for several different incubation times at room temperature. The shellac NPs were not loaded with BRB. The ratio of shellac : ODTAB in the NPs is fixed to 5 : 1. The x-axis shows the variation of the shellac and ODTAB concentrations for these experiments.

Antimicrobial effect of ODTAB-coated BRB-loaded shellac NPs

Fig. 10A shows the antimicrobial activity of different concentrations of BRB loaded in shellac NPs coated with ODTAB on *C. reinhardtii* at different incubation times. Here the nanocarrier has cationic surface functionality due to the ODTAB coating and is loaded with encapsulated BRB. Note the difference with the non-coated BRB-loaded shellac NPs in Fig. 6B. This comparison shows that after changing the surface charge of the nanocarrier from negative (Fig. 6B) to positive (Fig. 10A) using ODTAB coating, the BRB-loaded shellac NPs became much more effective antimicrobial agents. After only 15 minutes of incubation, all algal cells were killed at concentrations from 0.003 wt% to 0.01 wt% encapsulated BRB, and the algal cell viability was sharply reduced to 50% at 0.00005 wt% of encapsulated BRB. After 2 hours, the cell viability decreased significantly about 75% at 0.001 wt% of BRB loaded in ODTAB-coated shellac NPs. Fig. 10B shows the comparison among the antimicrobial activities of 0.0001 wt% encapsulated BRB, 0.0001 wt% free BRB, 0.0005 wt% shellac NPs coated with 0.0001 wt% ODTAB (no BRB), 0.0001 wt% BRB encapsulated in shellac NPs coated with 0.0001 wt% ODTAB, and 0.0001 wt% pure ODTAB. As it can be seen that there was an increase in the antimicrobial activity for the encapsulated BRB after being coated with ODTAB in comparison with the free BRB. The likely reason behind the increase in the antimicrobial activity of BRB after coating of the nanocarrier with ODTAB is the positive surface charge which attracts the NPs to the negatively algal cell walls and allow high concentration of BRB to be locally

delivered on the cell, although the overall BRB concentration in the formulation is extremely low. These findings are supported by the SEM images in Fig. 10D–F of *C. reinhardtii* cells after incubating for 2 hours with 0.005 wt% of BRB loaded shellac NPs coated with 0.005 wt% ODTAB which indicate that the positively charged surface ODTAB-coated BRB-loaded shellac NPs are indeed attracted to the algal cell membrane, thus increasing the delivered amount of BRB directly on the cell membrane.

Our earlier test results presented Fig. 7 showed that free BRB and encapsulated BRB within non-coated shellac NPs do not have significant cytotoxic effect on *S. cerevisiae* due to its extra-thick yeast cell wall (200 nm) which is hard to penetrate by BRB even at relatively high concentrations. In Fig. 11A we show the antimicrobial activity of ODTAB-coated BRB-loaded shellac NPs upon incubation as a function of the encapsulated BRB concentration. After 15 minutes exposure time, the cell viability severely decreased from 99% at control to 25%, 17% and 11% at 0.005, 0.007, and 0.01 wt% of BRB loaded in shellac NPs coated with 0.005, 0.007, and 0.01 wt% ODTAB, respectively. After 4 hours all cells died at 0.007 wt% and 0.01 wt% BRB loaded shellac NPs coated with ODTAB. Fig. 11B gives the comparison among the antimicrobial activities of 0.001 wt% BRB–shellac NPs, 0.001 wt% free BRB, 0.005 wt% shellac NPs coated with 0.001 wt% ODTAB, 0.001 wt% BRB encapsulated in shellac NPs coated with 0.001 wt% ODTAB, and 0.001 wt% free ODTAB. It can be seen that after coating of the BRB-loaded shellac NPs with ODTAB, the activity against yeast also increased, although less than for algal cells. Free BRB solution and non-coated BRB-
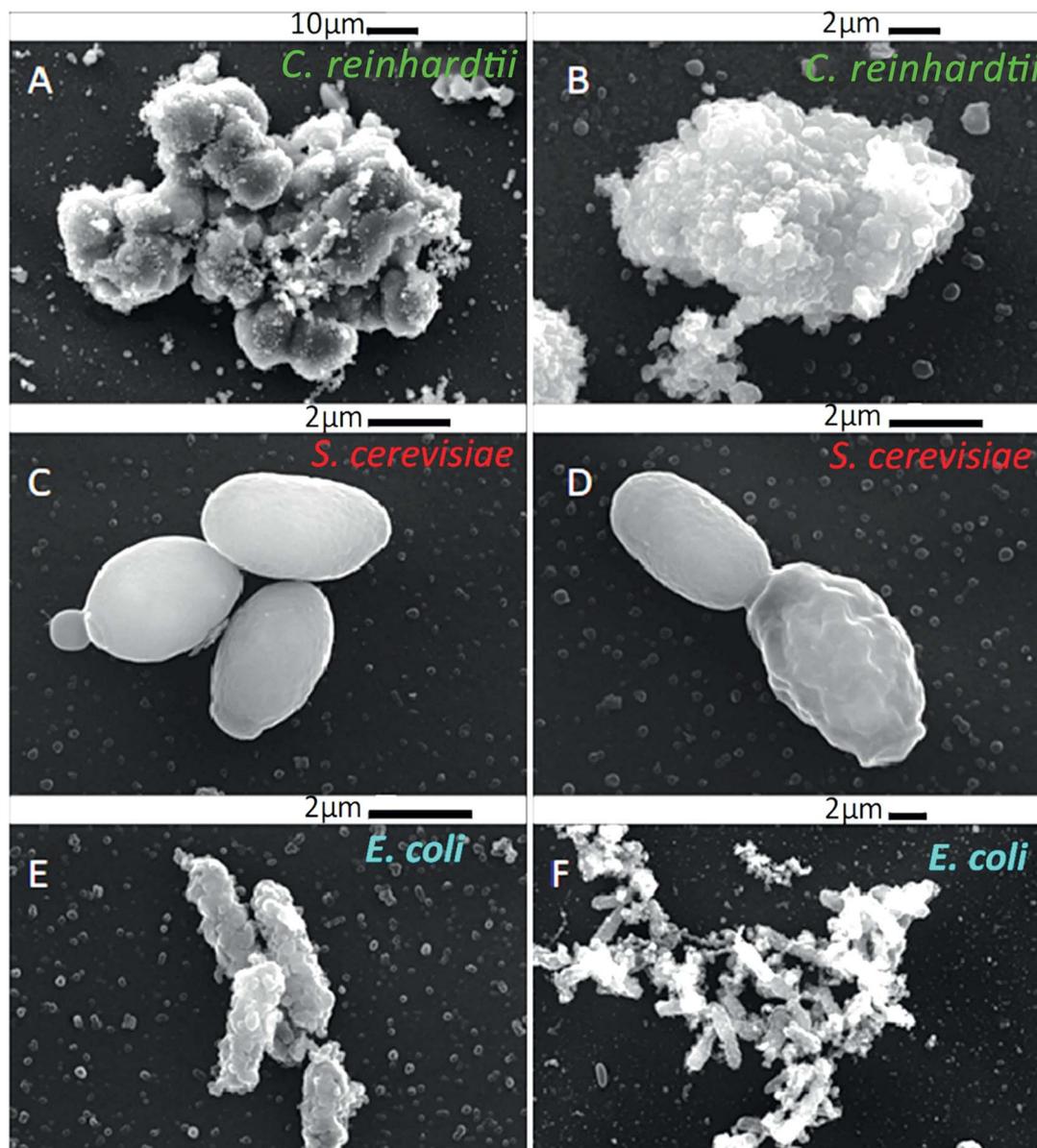
Fig. 9 SEM images of microbial cells with 0.025 wt% ODTAB–coated 0.125 wt% shellac NPs after 4 hours incubation at pH 5.5. (A) and (B) *C. reinhardtii*, (C) and (D) *S. cerevisiae* and (E) and (F) *E. coli* after 4 hours incubation at pH 5.5. The shellac NPs were not loaded with BRB.

loaded shellac NPs did not show any antimicrobial effect on yeast while the incubation with ODTAB-coated BRB-loaded shellac NPs caused a noticeable damage to yeast cell walls, which was also supported by the SEM images of the treated yeast cells presented in Fig. 11–F, compared with the control (Fig. 11C).

The antibacterial activity of BRB-loaded shellac NPs coated with ODTAB on *E. coli* cells was examined by incubating various concentration of ODTAB-coated BRB-loaded shellac NPs as shown in Fig. 12A. There is a marked increase of the antibacterial activity at concentrations of encapsulated BRB from 0.001 wt% to 0.01 wt% after 15 minutes of incubation, where the *E. coli* cell viability declined from 40×10^5 RLU (for the control) to (15, 13 and 11) $\times 10^5$ RLU at 0.005, 0.007 and 0.01 wt% overall concentration of BRB loaded in shellac NPs

coated with 0.008, 0.01 and 0.017 wt% ODTAB, respectively. After 1 hour the cell viability decreased strongly from 39×10^5 RLU to (4.3, 3.6, and 3.2) x10^5 RLU at 0.005, 0.007 and 0.01 wt% overall concentration of encapsulated BRB coated with 0.008, 0.01 and 0.017 wt% ODTAB respectively. We found that the cell viability decreased extremely sharply after 2 hours of incubation in this treatment and most cells died at concentration higher than 0.005 wt% of encapsulated BRB in ODTAB-coated shellac NPs. Fig. 12(B) shows a comparison between the effects of free BRB, non-coated and ODTAB-coated BRB-loaded shellac NPs upon incubation with *E. coli* as well as the antibacterial activity of ODTAB-coated non-loaded shellac NPs (no BRB) and free ODTAB. Similarly to the case of algal and yeast cells, the non-coated BRB-loaded shellac NPs showed lower activity against *E. coli* than the free BRB after 2 hours of incubation time,
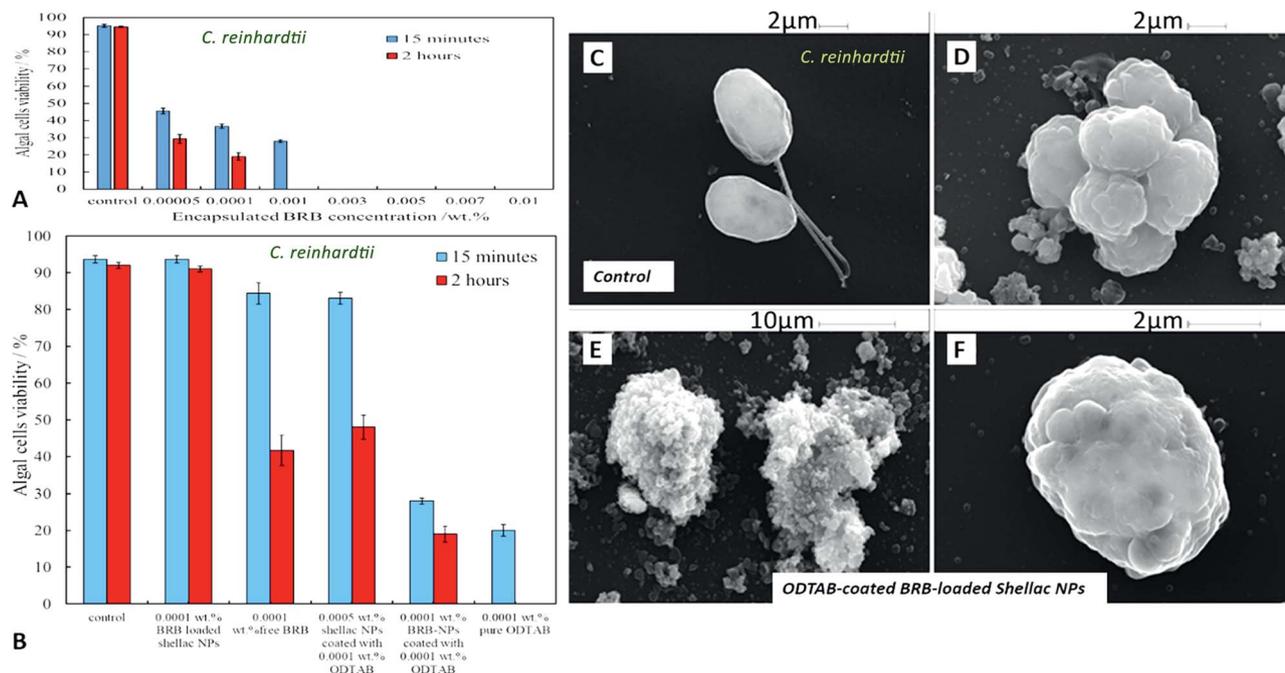
Fig. 10 (A) The viability of *C. reinhardtii* upon incubation at pH 5.5 with aqueous solutions of different concentrations of BRB encapsulated in ODTAB-coated BRB-loaded shellac NPs. The solutions were prepared from 0.05 wt% BRB (shellac) NPs stock solution coated with 0.05 wt% ODTAB. (B) The *C. reinhardtii* viability upon incubation with 0.0001 wt% encapsulated BRB in shellac NPs, 0.0001 wt% free BRB, 0.0005 wt% shellac NPs coated with 0.0001 wt% ODTAB, 0.0001 wt% BRB−NPs coated with 0.0001 wt% ODTAB, and 0.0001 wt% pure ODTAB at pH 5.5 and at room temperature. (C)−(F) SEM images of *C. reinhardtii* whereby (C) represent the control sample. (D)−(F) *C. reinhardtii* incubated with 0.005 wt% BRB loaded shellac NPs coated with 0.005 wt% ODTAB after 2 hours at room temperature.
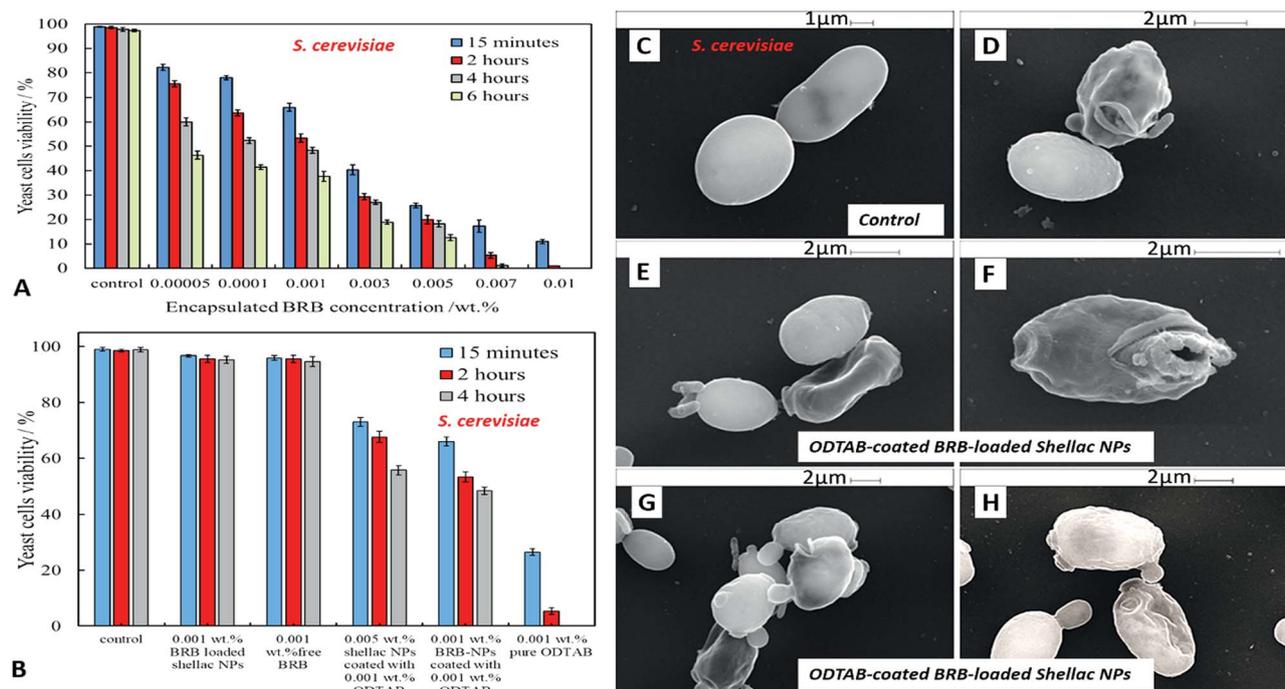

Fig. 11 (A) The viability of *S. cerevisiae* upon incubation at pH 5.5 with different amounts of BRB-loaded shellac NPs coated with ODTAB at room temperature at different incubation time. The solutions were prepared from 0.05 wt% BRB (shellac) NPs stock solution coated with 0.05 wt% ODTAB. (B) The yeast cells viability upon incubation with 0.001 wt% BRB−NPs, 0.001 wt% free BRB, 0.005 wt% shellac NPs coated with 0.001 wt% ODTAB, 0.001 wt% BRB−(shellac NPs) coated with 0.001 wt% ODTAB, and 0.001 wt% pure ODTAB. (C) SEM images of the control sample of *S. cerevisiae*, (D)−(H) SEM images of *S. cerevisiae* incubated with 0.01 wt% BRB loaded in shellac NPs coated with 0.01 wt% ODTAB after 2 hours at room temperature.
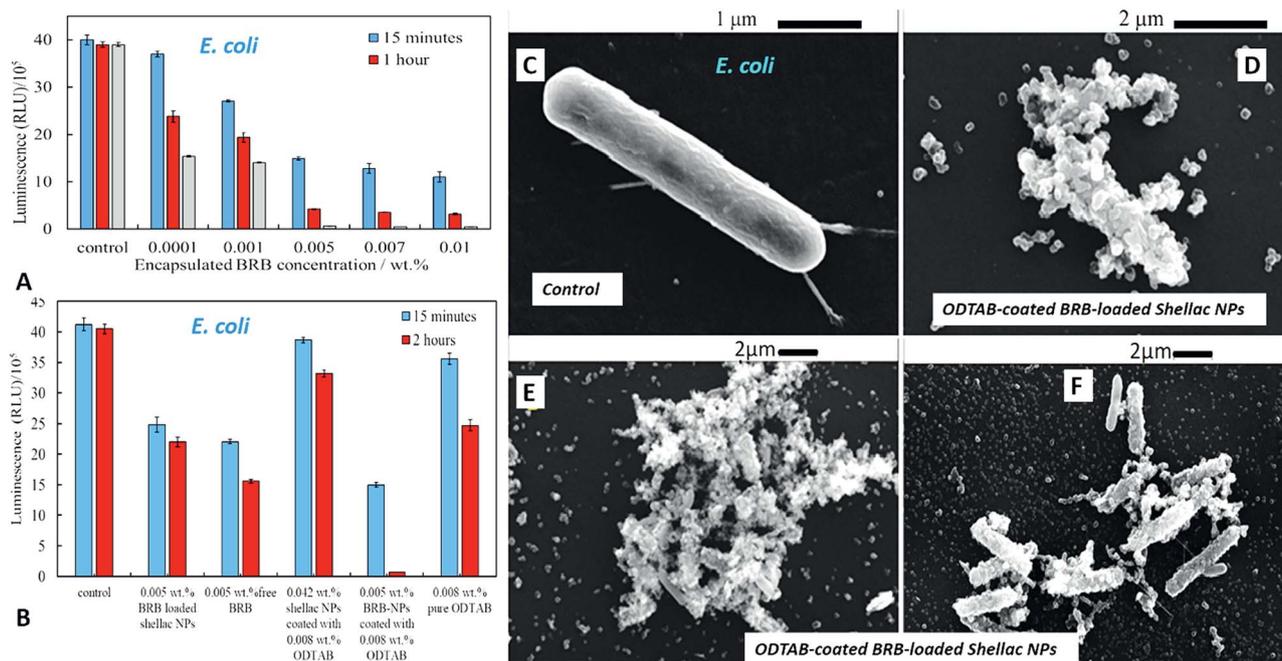
Fig. 12 (A) The antimicrobial activity of different concentrations of BRB–loaded shellac NPs coated with ODTAB against *E. coli*. These solutions were prepared from 0.03 wt% BRB loaded shellac NPs coated with 0.05 wt% ODTAB as stock solution. (B) The relative luminescence unit representing the *E. coli* viability upon incubation with 0.005 wt% BRB loaded in shellac NPs coated with 0.008 wt% ODTAB in regards to the antimicrobial activity of free BRB and BRB-loaded shellac NPs and the cytotoxic effect of pure ODTAB and ODTAB-coated shellac NPs. The incubation was also achieved through incubating each concentration with a fixed amount of *E. coli* at pH 5.5. (C)–(F) SEM images of *E. coli* whereby (C) represent the control sample, (D) and (E) *E. coli* incubated with 0.01 wt% BRB-loaded in shellac NPs coated with 0.017 wt% ODTAB (F) *E. coli* incubated with 0.005 wt% BRB loaded in shellac NPs coated with 0.008 wt% ODTAB after 2 hours.

whereas, ODTAB-coated BRB-loaded shellac NPs showed much stronger antibacterial effect due to their positive surface charge. In comparison, a considerable increase in the antibacterial activity was observed after incubating *E. coli* with 0.005 wt% BRB loaded in ODTAB-coated shellac NPs at the same incubation time. SEM images of the non-treated (Fig. 12C) and the treated *E. coli* cells shown in Fig. 12D–F show how the ODTAB-coated shellac NPs loaded with BRB have completely covered the surface of the cells after 2 hours incubation which amplifies their antimicrobial effect.

In Table 1 we compare qualitatively the effect of shellac NPs and shellac NPs-encapsulated BRB and the ODTAB-coated shellac NPs on the studied microorganisms including *C. reinhardtii* microalgae, yeast and *E. coli* (see Fig. 9B, 10B and 11B for quantitative comparison). The results showed that shellac NPs did not express significant antimicrobial effect on these microorganisms except a very weak effect on the microalgae due to the presence of P407 which is used to sterically stabilise our shellac NPs. Free BRB showed moderate antimicrobial effect on the microalgae and *E. coli*, but not on yeast. After encapsulating BRB within shellac NPs its effect was reduced due to the interaction between the cationic BRB and anionic shellac NPs which delays the drug release. Besides, the negatively charged shellac NPs are repelled by the negatively charged microbial cell walls and this causes the BRB to be released away from the cell membrane. To overcome this problem, the nanocarriers loaded with BRB were coated with cationic surfactant ODTAB to change

their charge from negative to positive; this water-insoluble surfactant has been chosen in order to maintain the stability of P407-coated shellac NPs. The antimicrobial effect of encapsulated BRB coated with ODTAB increased very strongly due to the electrostatic attraction between the ODTAB-coated encapsulated BRB and the cell membranes. Thus, a high concentration of released BRB is delivered directly on the cell membranes and kills the cells despite the lower overall concentration of BRB released in the aqueous media. Shellac NPs loaded with BRB and coated with ODTAB showed the strongest cytotoxic effect on the microalgae cells, and slightly less on *E. coli* and yeast, which

Table 1 The cytotoxicity effect of each component on *C. reinhardtii*, yeast, and *E. coli* which represented by (++++: very strong, +++: strong, ++: medium, and +: weak)

Nanocarrier component	Antimicrobial effect on		
	C. reinhardtii	Yeast	*E. coli*
Shellac NPs stabilised with P407	+	+	+
Shellac NPs stabilised with P407 and coated ODTAB	+	+	+
Free BRB	+++	+	+++
Shellac NPs loaded with BRB and stabilised with P407	++	+	++
Shellac NPs loaded with BRB, stabilised with P407 and coated with ODTAB	++++	+++	++++

is attributed to the larger thickness of their cell membranes. The ODTAB-coated shellac NPs with encapsulated BRB expressed cytotoxicity about 20 times higher than the free BRB on algae and about 5 times higher on yeast and *E. coli*. On the other hand, the cytotoxic effect of the shellac NPs coated with ODTAB but without being loaded with BRB is very weak, *i.e.* the ODTAB is not the main contributor for the nanocarrier anti-microbial action rather than serving to facilitate the nanocarrier adhesion to the cells and achieve direct delivery.

Conclusions and outlook

We have designed and developed a universal and very efficient nanocarrier for antimicrobial agents based on shellac, which is a natural and biodegradable material. We demonstrate the design and the application of this approach to encapsulate and deliver berberine chloride (BRB). The nanocarrier was formulated and loaded with antimicrobial agent in two steps: (i) the first step involved controlled precipitation of aqueous ammonium shellac salts by a simultaneous pH change from 8 to 5 and adsorption of surface active polymer (P407) in the presence of the active antimicrobial component. In this step, the drug-loaded shellac NPs were formed spontaneously and simultaneously coated with a sterically stabilizing polymer, which allowed them to maintain their stability and ensure long shelf-life. Stable shellac NPs were produced at pH 5 with a particle hydrodynamic diameter of 66 ± 5 nm with zeta potential −18 ± 8 mV. (ii) The second step in the nanocarrier fabrication involved charge-reversing of the produced shellac NPs by doping their surface with an insoluble cationic surfactant (ODTAB), which gave them a positive surface charge in order to promote the nanocarrier adhesion to the negatively charged cell membranes of typical bacterial cells. Physical and chemical parameters such as the effect of different concentrations of the surface active polymer as well as the BRB concentrations were studied on the size distribution of the produced nanocarriers and their zeta potential. Optimal nanocarrier stability was obtained at a fixed concentration ratio of 0.25 wt% : 0.2 wt% of shellac : P407. Using 0.01–0.07 wt% concentration range of BRB with 0.25 wt% shellac at pH 5 to be encapsulated within shellac NPs we achieved maximum encapsulation efficiencies of 60% for BRB. The interaction between the NPs and the antimicrobials was characterized using FTIR and UV-visible techniques. We studied the release profiles of BRB loaded in the developed shellac nanocarriers and characterised the effect of the BRB-loading on their size and zeta-potential.

We investigated the importance of the nanocarrier architecture on the antimicrobial activity of the loaded. We explored the antimicrobial activity of BRB-loaded shellac nanocarriers on microalgae, yeast and bacterial cells. Although the free BRB in aqueous solution had an antimicrobial effect on these microorganisms, the non-coated shellac nanocarriers with BRB showed a reduction in antimicrobial activity due to the electrostatic repulsion between the negatively charged shellac NPs and the negatively charged microbial cell membranes which did not allow the encapsulated BRB to be released near the cell wall. In addition to this, the attraction between the BRB cations and

the shellac matrix of the nanocarriers led to slow BRB release. However, upon ODTAB functionalization of the BRB-loaded shellac NPs, their surface charge changed from negative to positive. We found the optimum conditions where the functionalised shellac nanocarriers become cationic and still maintained their stability due to steric interactions of the P407 layer. Consequently, the antimicrobial activity of these ODTAB-coated shellac NPs loaded with BRB showed a very significant increase in the antimicrobial effect of BRB compared with the equivalent overall concentration free BRB in solution. This effect was due to the strong electrostatic adhesion with the cell membrane which allowed the antimicrobial agents to be released directly into the microbial cell. This type of versatile surface-functionalised shellac nanocarriers can be potentially applied to boost the action for a range of low-molecular weight antimicrobial agents. Similar strategy could also be universally applied for enhancing the action of topical antibiotics and antifungal agents and could be used across different therapies to fight antimicrobial resistance.

Conflicts of interest

There are no conflicts of interest to declare.

Acknowledgements

Notes and references

1 H. Hillaireau and C. Patrick, *Cell. Mol. Life Sci.*, 2009, **66**, 2873–2896.

2 A. F. Halbus, T. S. Horozov and V. N. Paunov, *Adv. Colloid Interface Sci.*, 2017, **249**, 134–148.

3 A. A. K. Das and V. N. Paunov, *Microbiologist*, June 2014, pp. 16–19, https://issuu.com/societyforappliedmicrobiology/docs/2014_06_microbiologist.

4 C. Frangville, M. Rutkevicius, A. P. Richter, O. D. Velev, S. D. Stoyanov and V. N. Paunov, *ChemPhysChem*, 2012, **13**, 4235–4243.

5 A. P. Richter, J. S. Brown, B. Bharti, A. Wang, S. Gangwal, K. Houck, E. A. Cohen Hubal, V. N. Paunov, S. D. Stoyanov and O. D. Velev, *Nat. Nanotechnol.*, 2015, **10**, 817–823.

6 A. P. Richter, B. Bharti, H. B. Armstrong, J. S. Brown, D. Plemmons, V. N. Paunov, S. D. Stoyanov and O. D. Velev, *Langmuir*, 2016, **32**, 6468–6647.

7 M. J. Al-Awady, G. M. Greenway and V. N. Paunov, *RSC Adv.*, 2015, **5**, 37044–37059.

8 M. Imanshahidi and H. Hosseinzadeh, *Phytother. Res.*, 2008, **22**, 999–1012.

9 K. C. Singhal, *Indian J. Exp. Biol.*, 1976, **14**, 345–347.

10 T. Satou, N. Akao, R. Matsuhashi, K. Koike, K. Fujita and T. Nikaido, *Biol. Pharm. Bull.*, 2002, **25**, 1651–1654.

11 C. L. Kuo, C. W. Chi and T. Y. Liu, *Cancer Lett.*, 2004, **203**, 127–137.

12 M. Tillhon, L. M. Guamán Ortiz, P. Lombardi and A. I. Scovassi, *Biochem. Pharmacol.*, 2012, **84**, 1260–1267.

13 C. V. Diogo, N. G. Machando, I. A. Barbosa, T. L. Serafim, A. Burgeiro and P. J. Oliveira, *Curr. Drug Targets*, 2011, **12**, 850–859.

14 W. Tan, Y. Li, M. Chen and Y. Wang, *Int. J. Nanomed.*, 2011, **6**, 1773–1777.

15 L. Tan, G. Li, J. Chen, W. Su and K. Rong, *J. Pract. Med. Technol.*, 2007, **14**, 1385–1386.

16 M. Xue, M.-x. Yang, W. Zhang, X.-m. Li, D.-h. Gao, Z.-m. Ou, Z.-p. Li, S.-h. Liu, X.-j. Li and S.-y. Yang, *Int. J. Nanomed.*, 2013, **8**, 4677–4687.

17 S. Wang, T. Chen, R. Chen, Y. Hu, M. Chen and Y. Wang, *Int. J. Pharm.*, 2012, **430**, 238–246.

18 L. Wang, H. Li, S. Wang, R. Liu, Z. Wu, C. Wang, Y. Wang and M. Chen, *AAPS J.*, 2014, **15**, 834–844.

19 M. Khemani, M. Sharon and M. Sharon, *ISRN Nanotechnol.*, 2012, **2012**, 1–9.

20 R. Kapoor, S. Singh, M. Tripathi, P. Bhatnagar, P. Kakkar and K. C. Gupta, *PLoS One*, 2014, **9**, e89124.

21 M. J. Al-Awady, A. Fauchet, G. M. Greenway and V. N. Paunov, *J. Mater. Chem. B*, 2017, **5**, 7885–7897.

22 S. Limmatvapirat, C. Limmatvapirat, M. Luangtana-Anan, J. Nunthanid, T. Oguchi, Y. Tozuka, K. Yamamoto and S. Puttipipatkhachorn, *Int. J. Pharm.*, 2004, **278**, 41–49.

23 M. F. Ansari and D. N. Goswami, *Pigm. Resin Technol.*, 2006, **35**, 183–187.

24 A. Nevin, D. Comelli, G. Valentini and R. Cubeddu, *Anal. Chem.*, 2009, **81**, 1784–1791.

25 A. Azouka, R. Huggett and A. Harrison, *J. Oral Rehabil.*, 1993, **20**, 393–400.

26 A. Harrison, R. Huggett and A. Azouka, *J. Oral Rehabil.*, 1995, **22**, 509–513.

27 B. T. Hoang-Dao, H. Hoang-Tu, L. Tran-Hung, J. Camps, G. Koubi and I. About, *Dent. Mater.*, 2008, **24**, 1001–1007.

28 B. T. Hoang-Dao, H. Hoang-Tu, N. N. Tran-Thi, G. Koubi, J. Camps and I. About, *J. Oral Rehabil.*, 2009, **36**, 124–131.

29 S. Y. Lee, K. L. Dangaran and J. M. Krochta, *J. Food Sci.*, 2002, **67**, 1121–1125.

30 J. Nickel and U. Riedel, *Biorelated Polymers*, 2001, 27–40.

31 S. Leick, M. Kott, P. Degen, S. Henning, T. Pasler, D. Suter and H. Rehage, *Phys. Chem. Chem. Phys.*, 2011, **13**, 2765–2773.

32 Y. Farag and C. S. Leopold, *Drug Dev. Ind. Pharm.*, 2011, **37**, 193–200.

33 S. A. Hamad, S. D. Stoyanov and V. N. Paunov, *Soft Matter*, 2012, **8**, 5069–5077.

34 D. Phan Thea, F. Debeautfort, D. Luu and A. Voilley, *J. Membr. Sci.*, 2008, **325**, 277–283.

35 R. D. Hagenmaier and P. E. Shaw, *J. Agric. Food Chem.*, 1991, **39**, 825–829.

36 W. H. Gardner and W. F. Whitmore, *Ind. Eng. Chem.*, 1929, **21**, 226–229.

37 S. I. F. Badawy, A. J. Gawronski and F. J. Alvarez, *Int. J. Pharm.*, 2001, **223**, 89–92.

38 A. R. Patel, D. S. Schatteman, W. H. De Vos and K. Dewettinck, *RSC Adv.*, 2013, **3**, 5324–5327.

39 S. Limmatvapirat, C. Limmatvapirat, S. Puttipipatkhachorn, J. Nuntanid and M. Luangtana-Anan, *Eur. J. Pharm. Biopharm.*, 2007, **67**, 690–698.

40 L. M. Bellan, M. Pearsall, D. M. Cropek and R. Langer, *Adv. Mater.*, 2012, **24**, 5187–5191.

41 A. R. Patel, E. Dorst, J. Seijen ten Hoorn and K. P. Velikov, *Soft Matter*, 2013, **9**, 6747–6751.

42 W. H. Gardner and W. F. Whitmore, *Ind. Eng. Chem.*, 1929, **21**, 226–229.

43 A. Patel, P. Heussen, J. Hazekamp and K. P. Velikov, *Soft Matter*, 2011, **7**, 8549–8555.

44 P. Kraisit, S. Limmatvapirat, J. Nunthanid, P. Sriamornsak and M. Luangtana-anan, *Pharm. Dev. Technol.*, 2013, **18**, 686–693.

45 K. Krause and R. Müller, *Int. J. Pharm.*, 2001, **223**, 89–92.

46 A. A. K. Das, M. M. N. Esfahani, O. D. Velev, N. Pamme and V. N. Paunov, *J. Mater. Chem. A*, 2015, **3**, 20698–20707.

47 *Cold Spring Harb. Protoc.*, 2006, **2006**, pdb.rec8194, http://cshprotocols.cshlp.org/.

48 *Cold Spring Harb. Protoc.*, 2009, **2009**, pdb.rec11945, http://cshprotocols.cshlp.org/.

49 D. B. Sofia Papadimitriou, *J. Controlled Release*, 2009, **138**, 177–184.

50 Z. C. Xiaodan Zhou, *Arch. Pharmacal Res.*, 2015, **38**, 2193–2200.

51 H. R. Patel, R. P. Patel and M. Patel, *Int. J. PharmTech Res.*, 2009, **1**, 299–303.

52 J. Lu, H. Wang, J. Huang, G. Li, Q. Wang, W. Xu, Y. Chen, K. Zhang and J. Wang, *Fitoterapia*, 2014, **97**, 64–70.

53 V. Kunasekaran and K. Krishnamoorthy, *Int. J. Pharm. Pharm. Sci.*, 2015, **7**, 73–80.

54 M. Khemani, M. Sharon and M. Sharon, *ISRN Nanotechnol.*, 2012, **2012**, 1–9.

55 M.-L. Veyries, F. Faurisson, M.-L. Joly-Guillou and B. Rouveix, *Antimicrob. Agents Chemother.*, 2000, **44**, 1093–1096.

56 H. Yamada, N. Koike, T. Ehara and T. Matsumoto, *J. Infect. Chemother.*, 2011, **17**, 195–199.

57 M. Portoles, M. F. Refojo and F. L. Leong, *J. Biomed. Mater. Res.*, 1994, **28**, 303–309.

58 M. Mehra, J. Sheorain and S. Kumari, *AIP Conf. Proc.*, 2016, **1724**, 020060.

59 J. Yin, H. Xing and J. Ye, *Metab., Clin. Exp.*, 2008, **57**, 712–717.

60 J. A. Marin-Neto, B. C. Maciel, A. L. Secches and L. Gallo Junior, *Clin. Cardiol.*, 1988, **11**, 253–260.

61 F. Y. Fung and Y. C. Linn, *Evidence-based complementary and alternative medicine*, eCAM, 2015, vol. 2015, p. 425037.

62 J. Bateman, R. D. Chapman and D. Simpson, *Scott. Med. J.*, 1998, **43**, 7–15.

63 M. Cernakova and D. Kostalova, *Folia Microbiol.*, 2002, **47**, 375–378.